Supplement of Geosci. Model Dev., 13, 5345–5366, 2020
https://doi.org/10.5194/gmd-13-5345-2020-supplement

Geoscientific Model Development
Open Access
EGU

Supplement of

Land surface model influence on the simulated climatologies of temperature and precipitation extremes in the WRF v3.9 model over North America

Almudena García-García et al.

Correspondence to: Hugo Beltrami (hugo@stfx.ca)

Table S1. Information on the visited websites for retrieving data or detailed information.

Product	Website	Date of access
ETCCDI	https://www.climdex.org/learn/indices/	December, 2018
NA-CORDEX	https://www.earthsystemgrid.org/search/cordexsearch.html	December, 2018
NARR	https://nomads.ncdc.noaa.gov/data/narr/	August, 2017
ARW-WRF Version 3.9	http://www2.mmm.ucar.edu/wrf/users/download/get_source.html	August, 2017

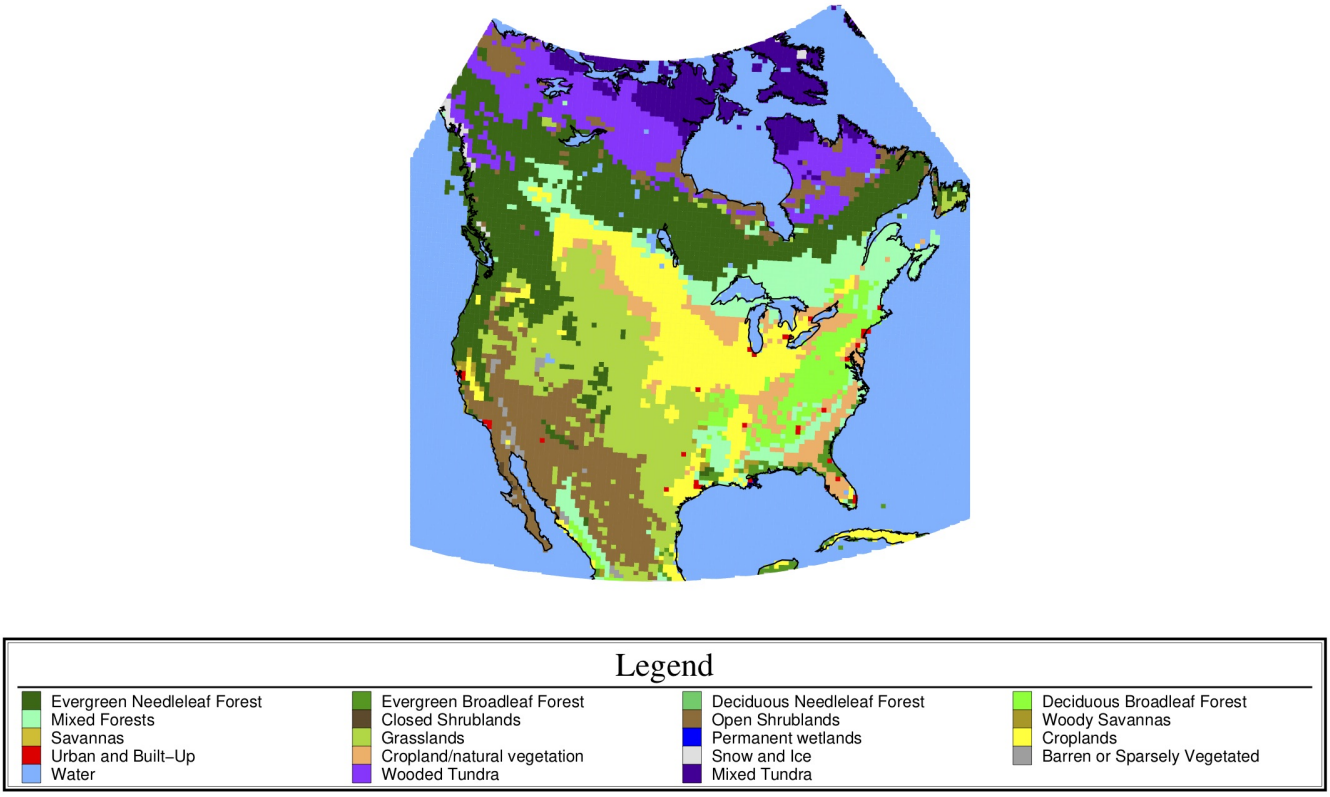

Figure S1. Land use categories used in all our four simulations with different LSM configurations. These land use categories are derived from the Moderate Resolution Imaging Spectroradiometer (MODIS, Barlage et al., 2005).

References

Barlage, M., Zeng, X., Wei, H., and Mitchell, K. E.: A global 0.05° maximum albedo dataset of snow-covered land based on MODIS observations, Geophysical Research Letters, 32, https://agupubs.onlinelibrary.wiley.com/doi/abs/10.1029/2005GL022881, 2005.

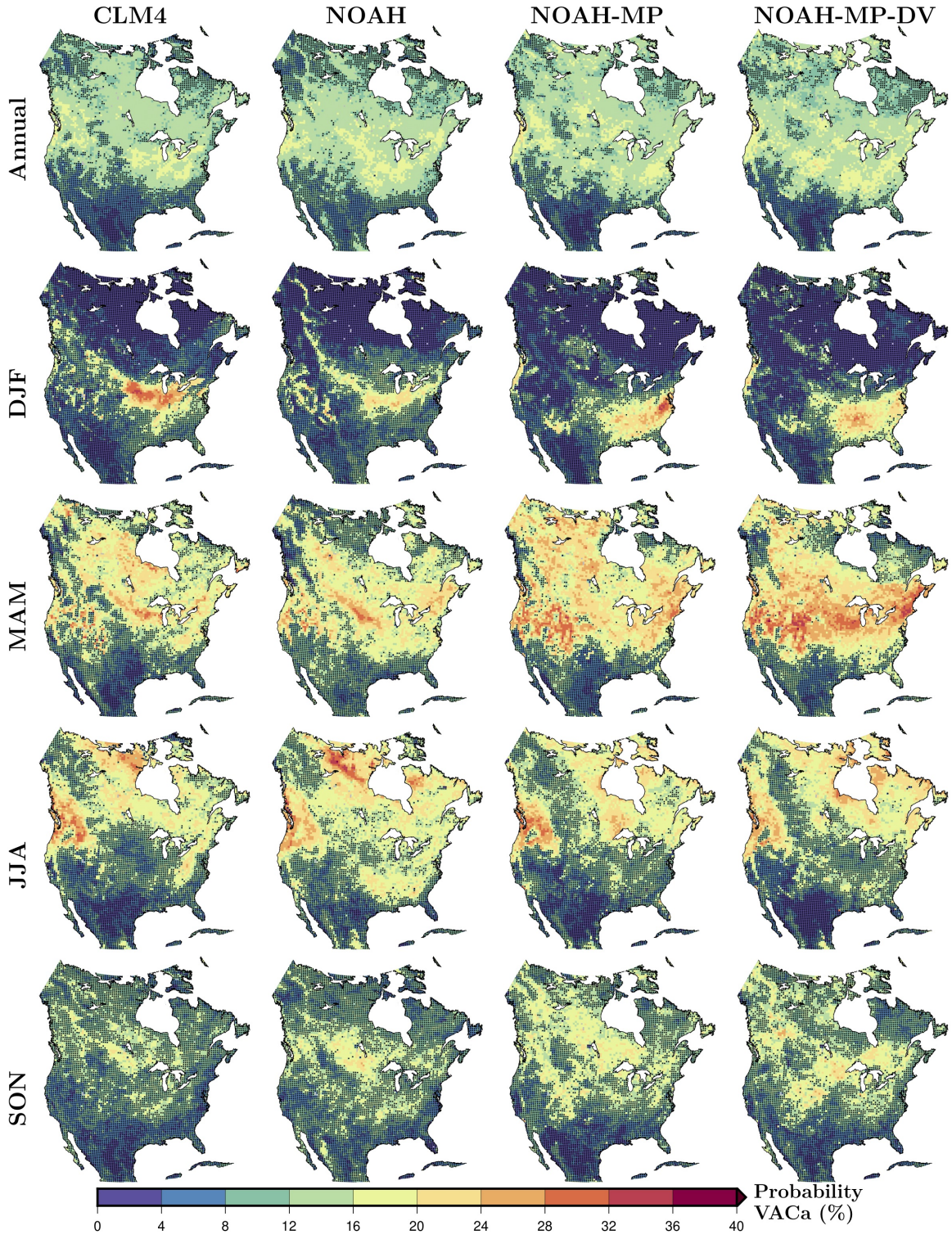

Figure S2. Frequency of occurrence for the VAC_a category associated with atmospheric control events for each simulation annually and seasonally; DJF, MAM, JJA and SON. Black dots in the maps indicate VAC values lower than the 95th percentile of the randomly generated series, and therefore areas with no significant probabilities.

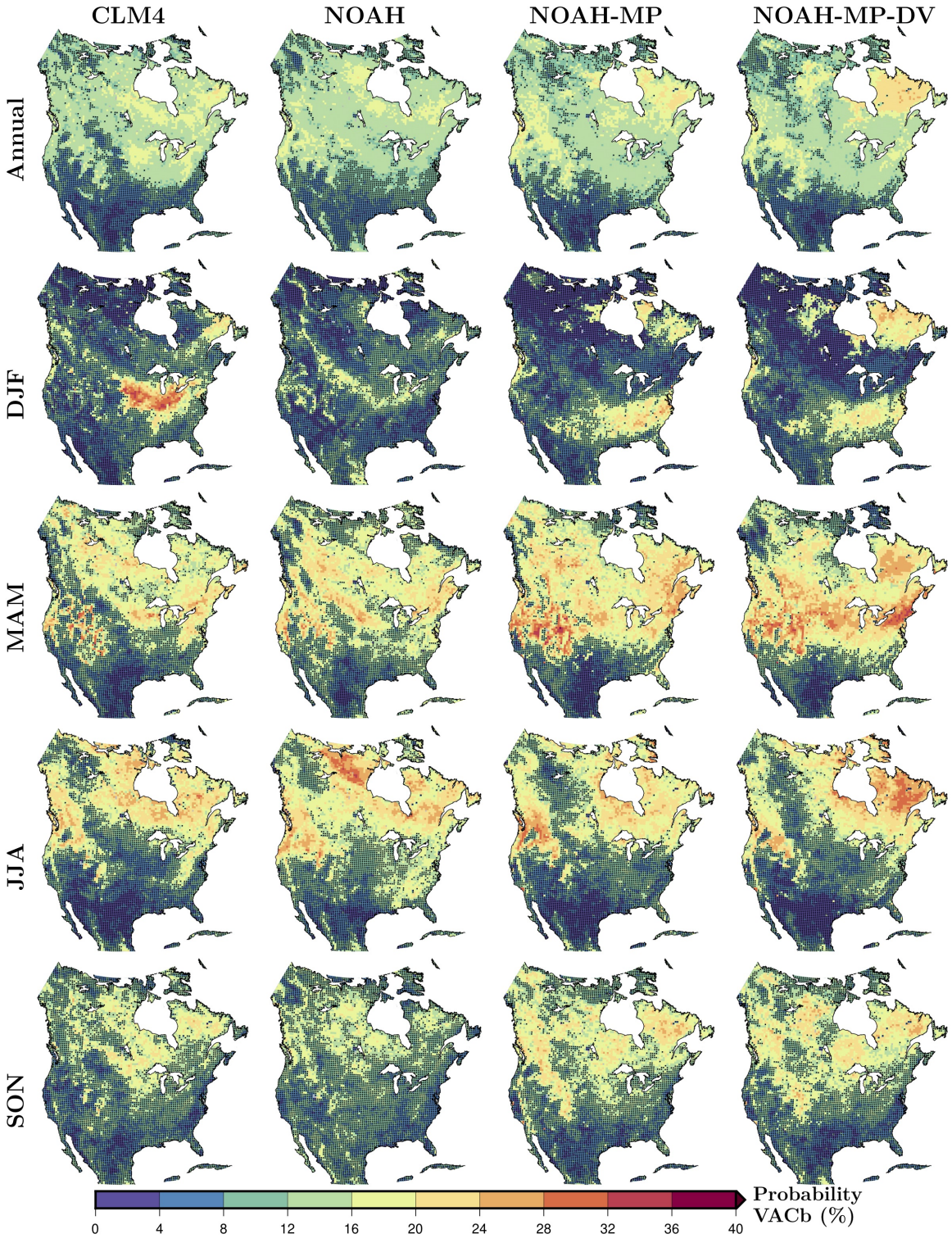

Figure S3. As in Figure S1 but for the VAC_b category.

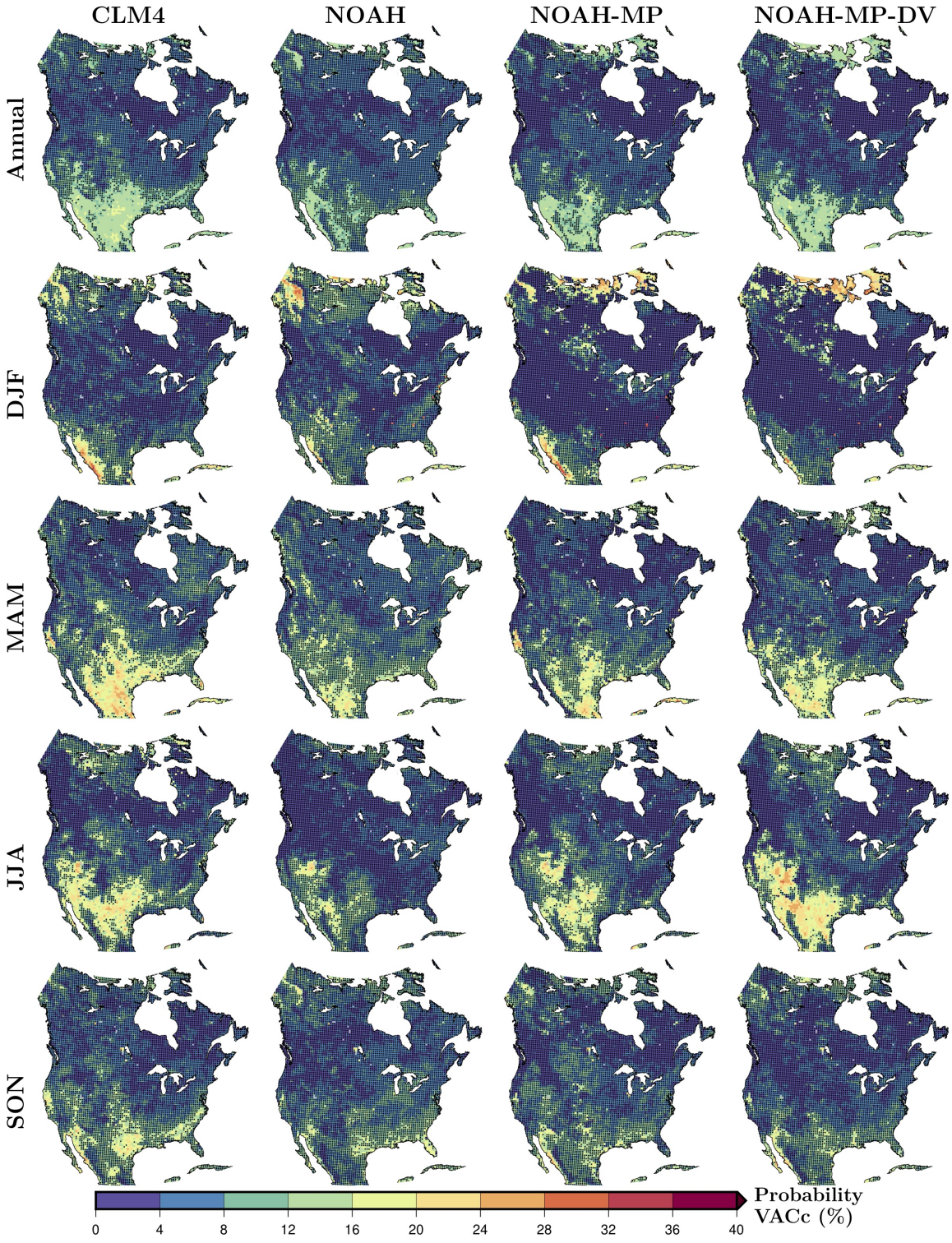

Figure S4. As in Figure S1 but for the VAC_c category.

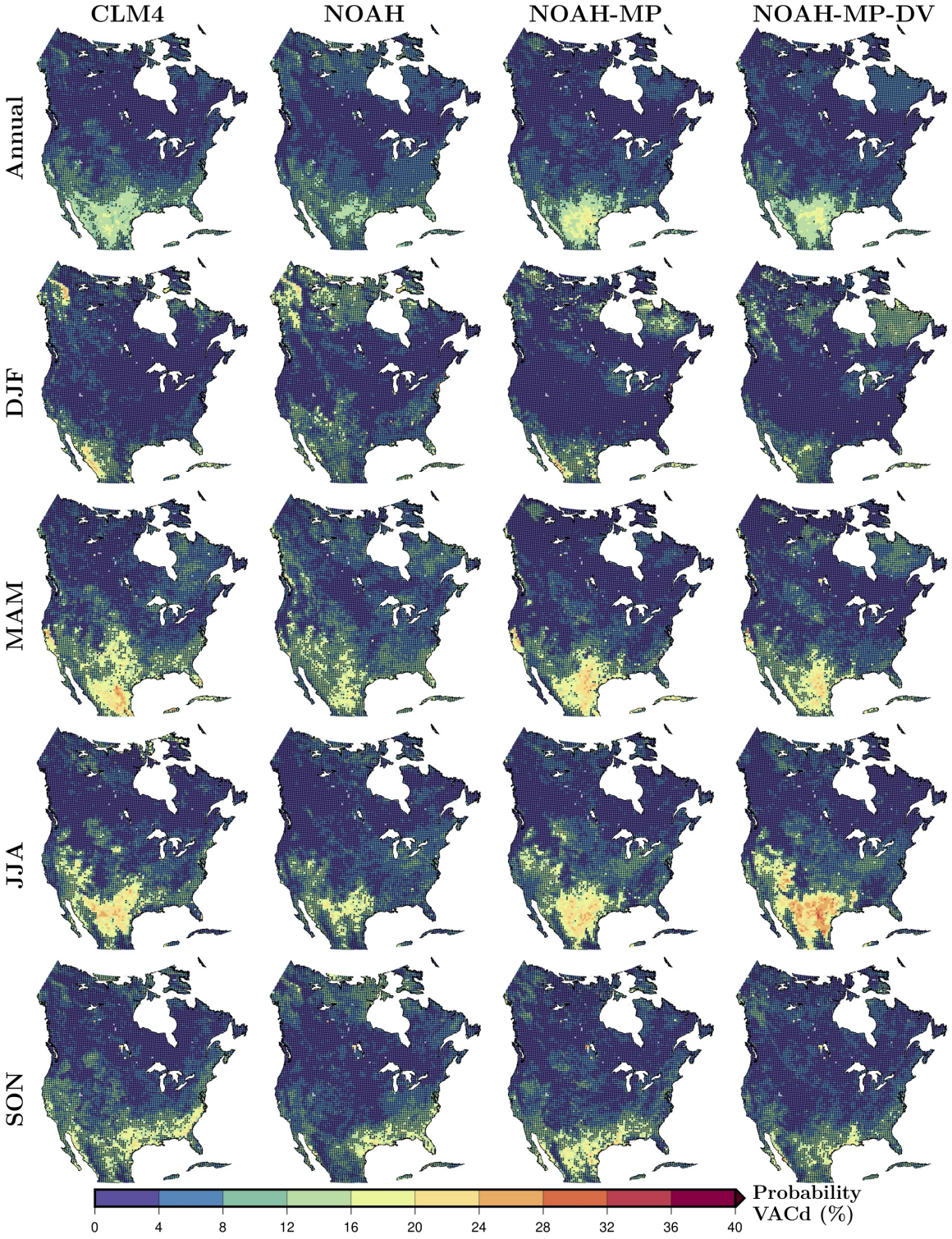

Figure S5. As in Figure S1 but for the VAC_d category.

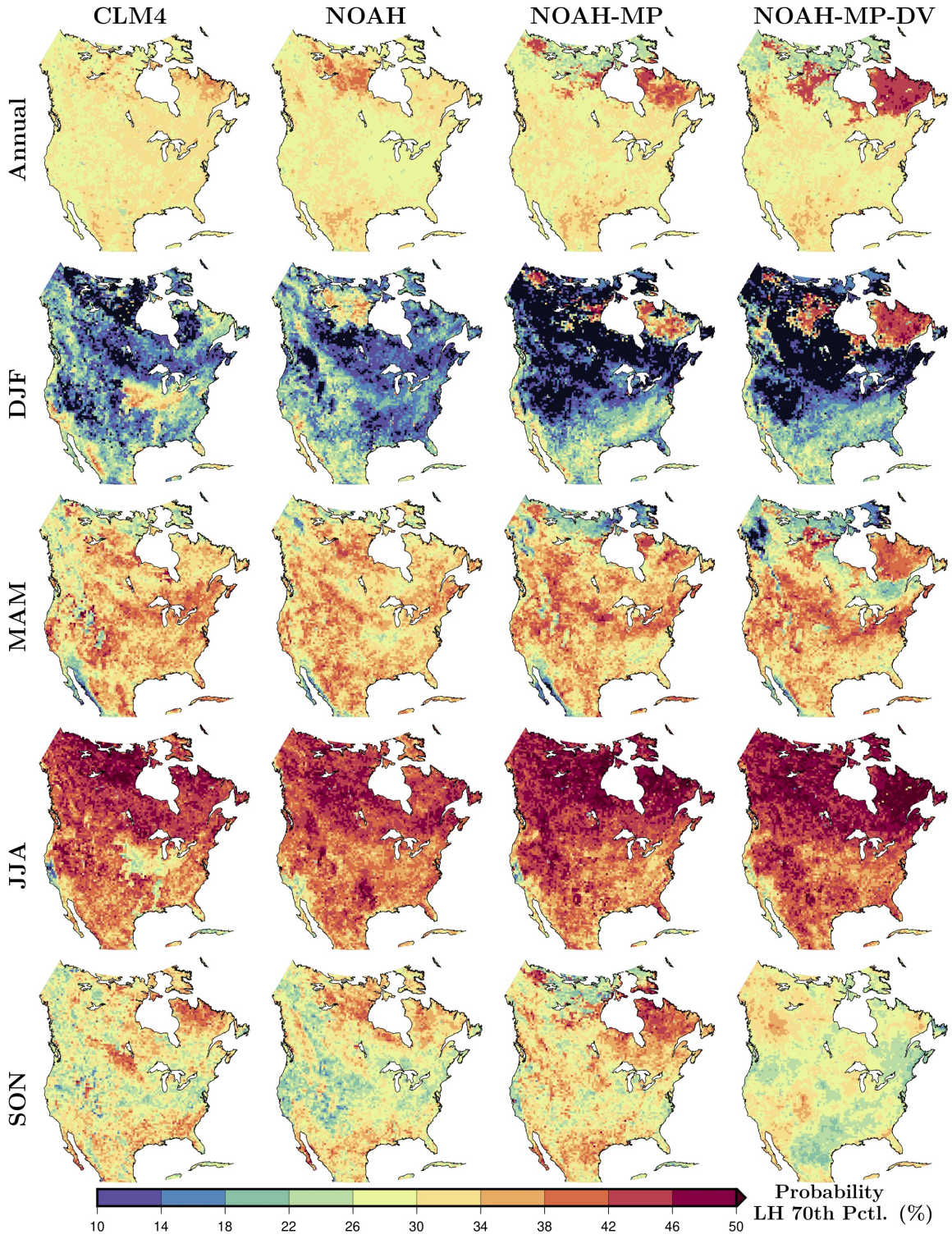

Figure S6. Frequency of occurrence for the extreme high latent heat flux for each simulation annually and seasonally; DJF, MAM, JJA and SON. Extreme high latent heat flux events are defined as values higher than the 70th percentile of the latent heat flux time series from 1980 to 2000 at each grid cell.

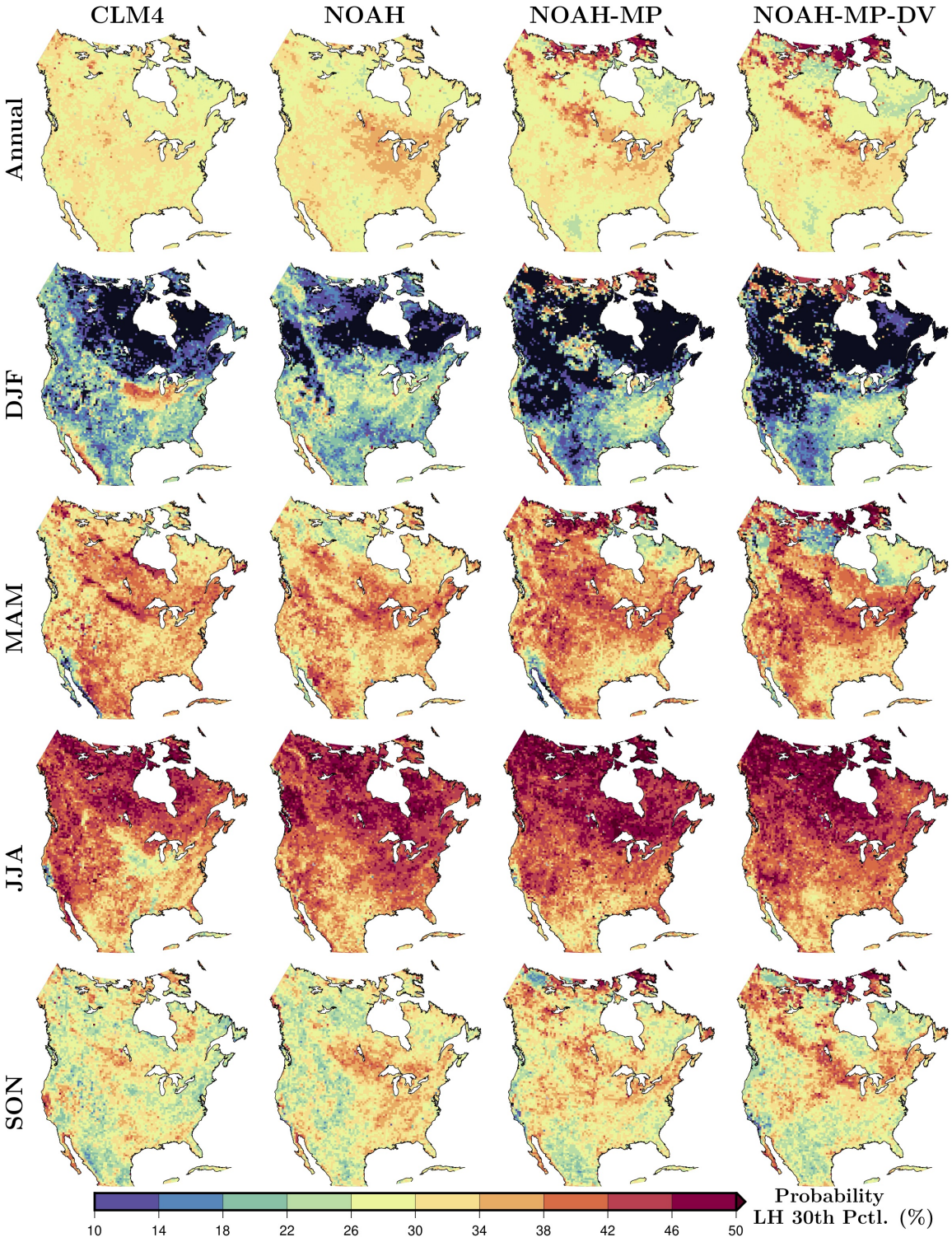

Figure S7. Frequency of occurrence for the extreme low latent heat flux for each simulation annually and seasonally; DJF, MAM, JJA and SON. Extreme high latent heat flux events are defined as values lower than the 30th percentile of the latent heat flux time series from 1980 to 2000 at each grid cell.

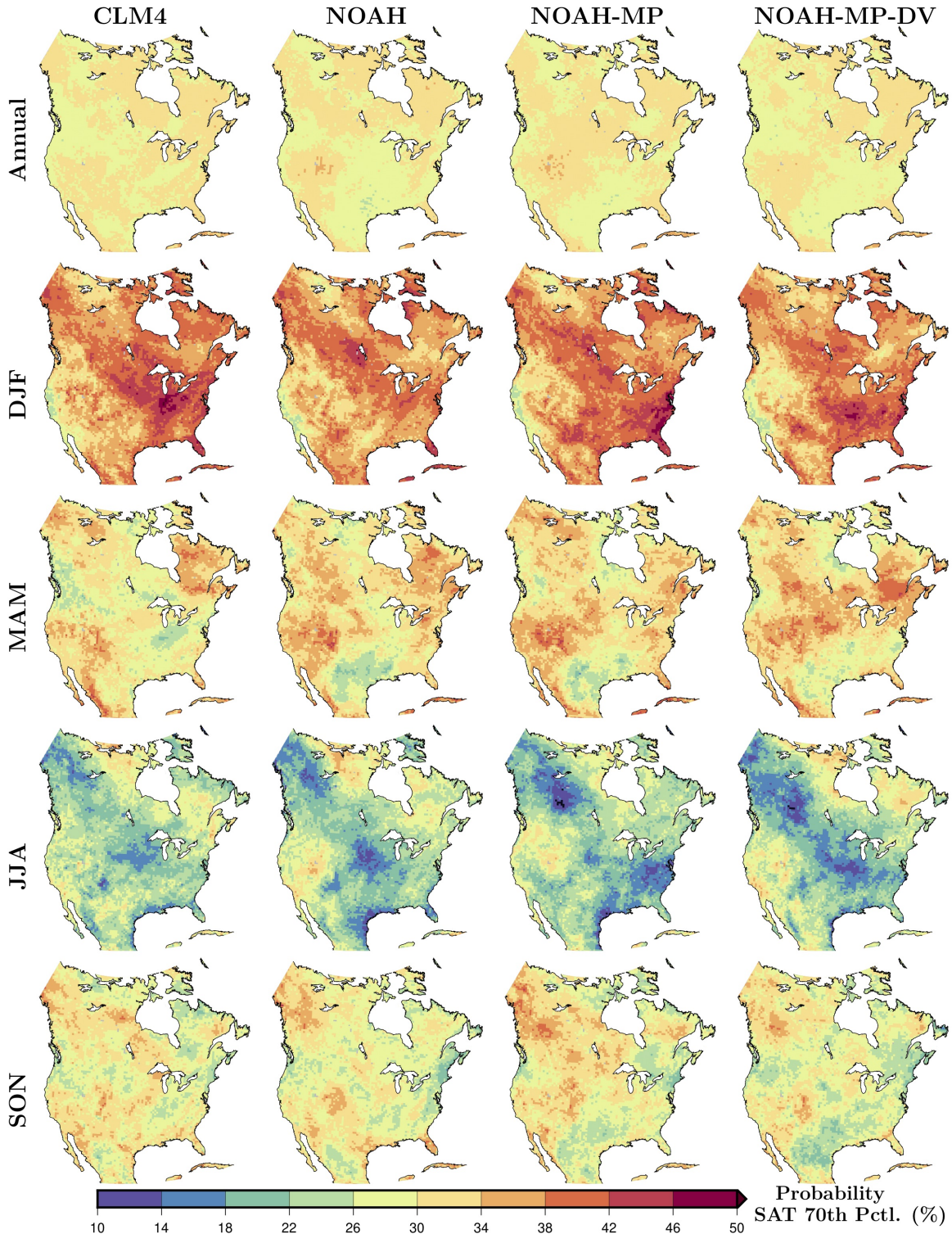

Figure S8. As in Figure S6 but for Surface Air Temperature (SAT.)

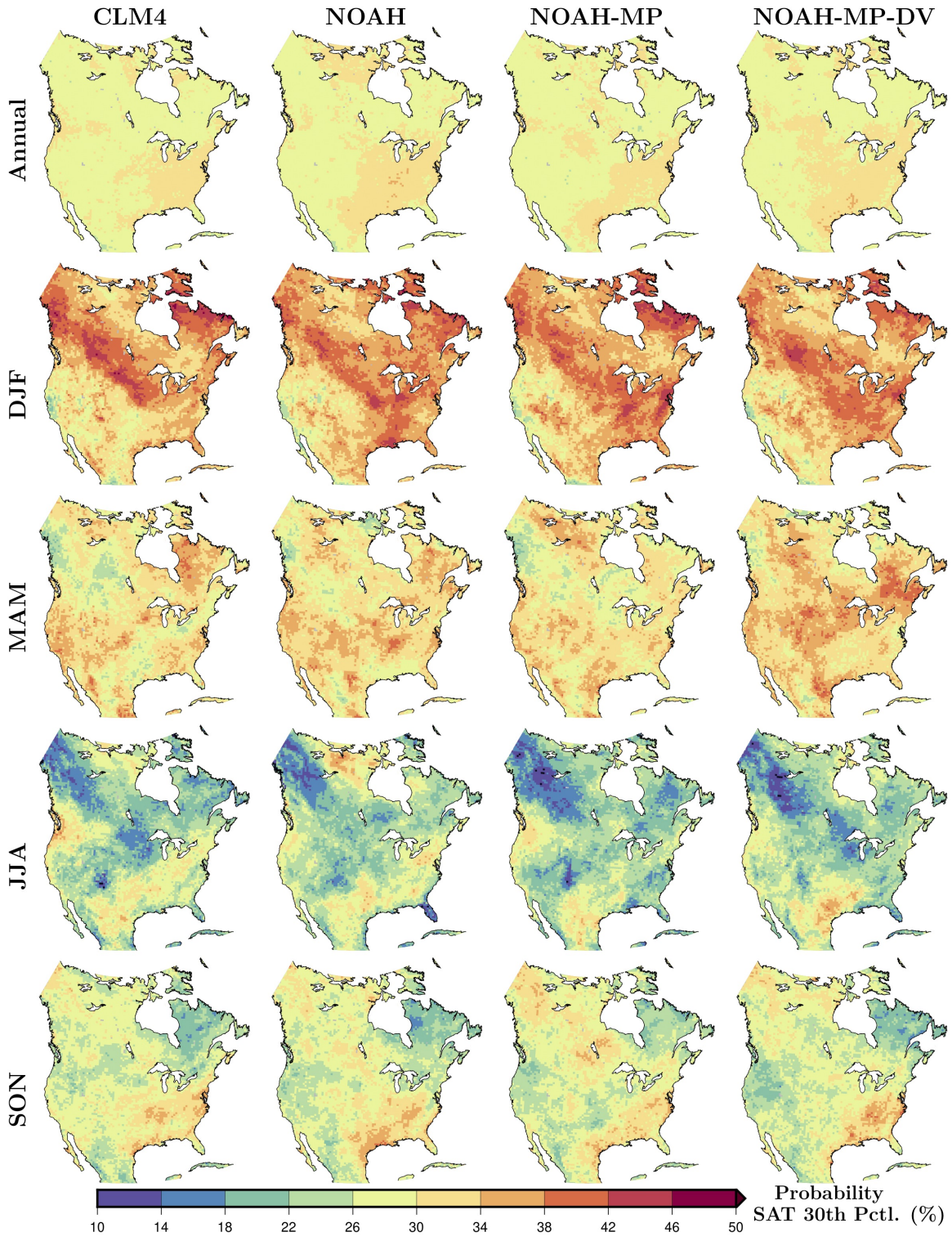

Figure S9. As in Figure S7 but for Surface Air Temperature (SAT.)

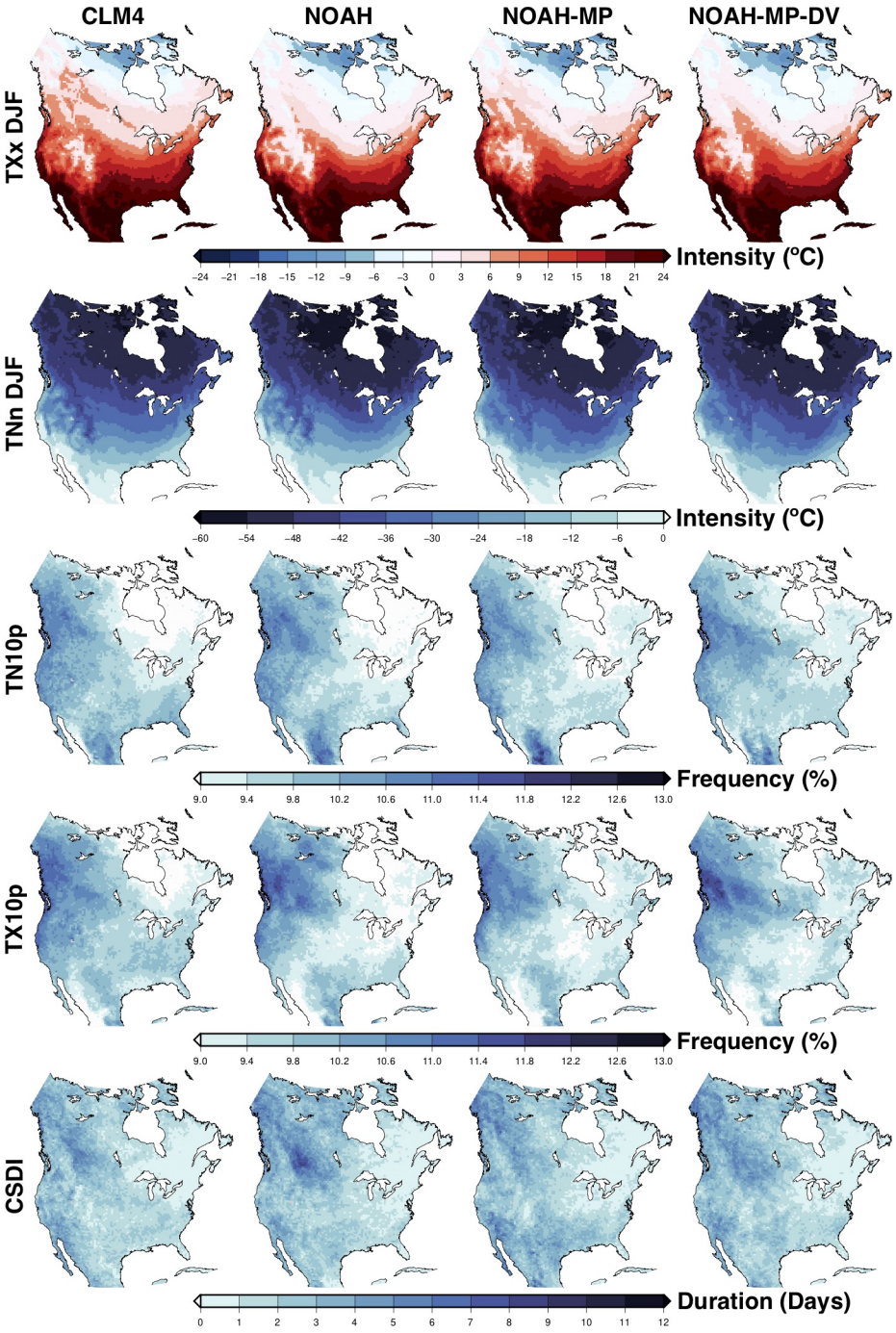

Figure S10. Climatologies of extreme indices associated with intensity, frequency, and duration of cold extreme temperature events for each simulation separately (Table 2). The indices are computed using the mean of each index from 1980 to 2012 for each simulation.

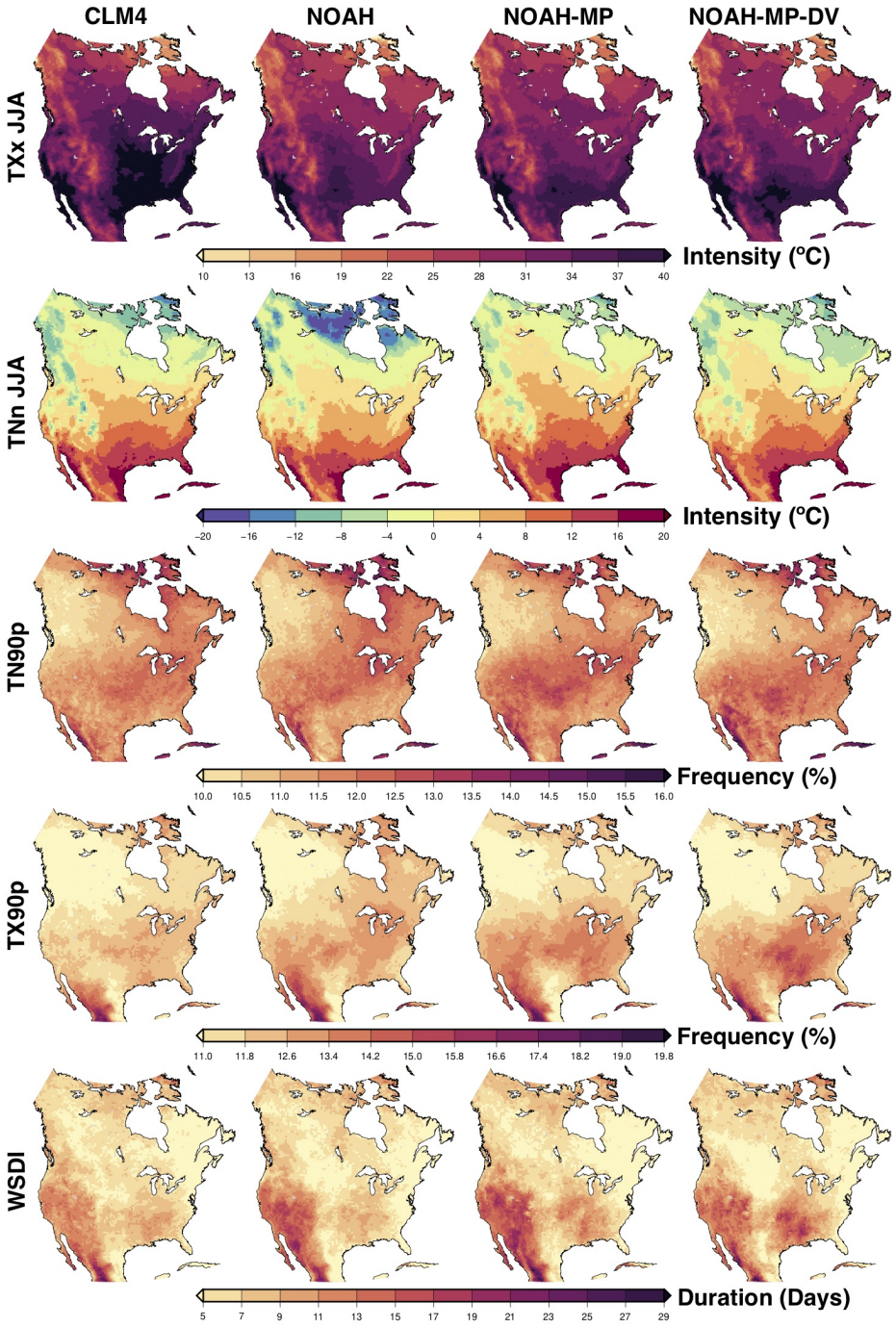

Figure S11. As in Figure S10 but for warm extreme temperature events.

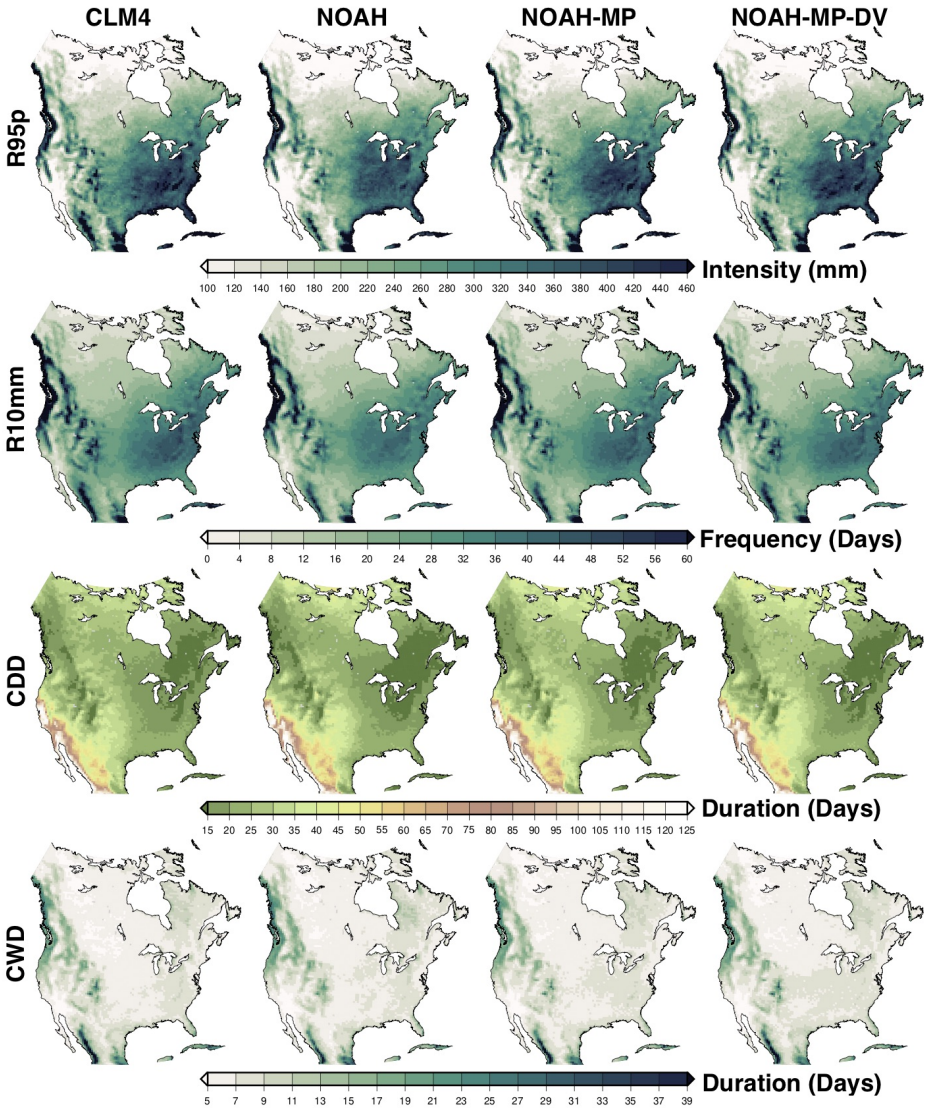

Figure S12. As in Figure S10 but for extreme precipitation events.

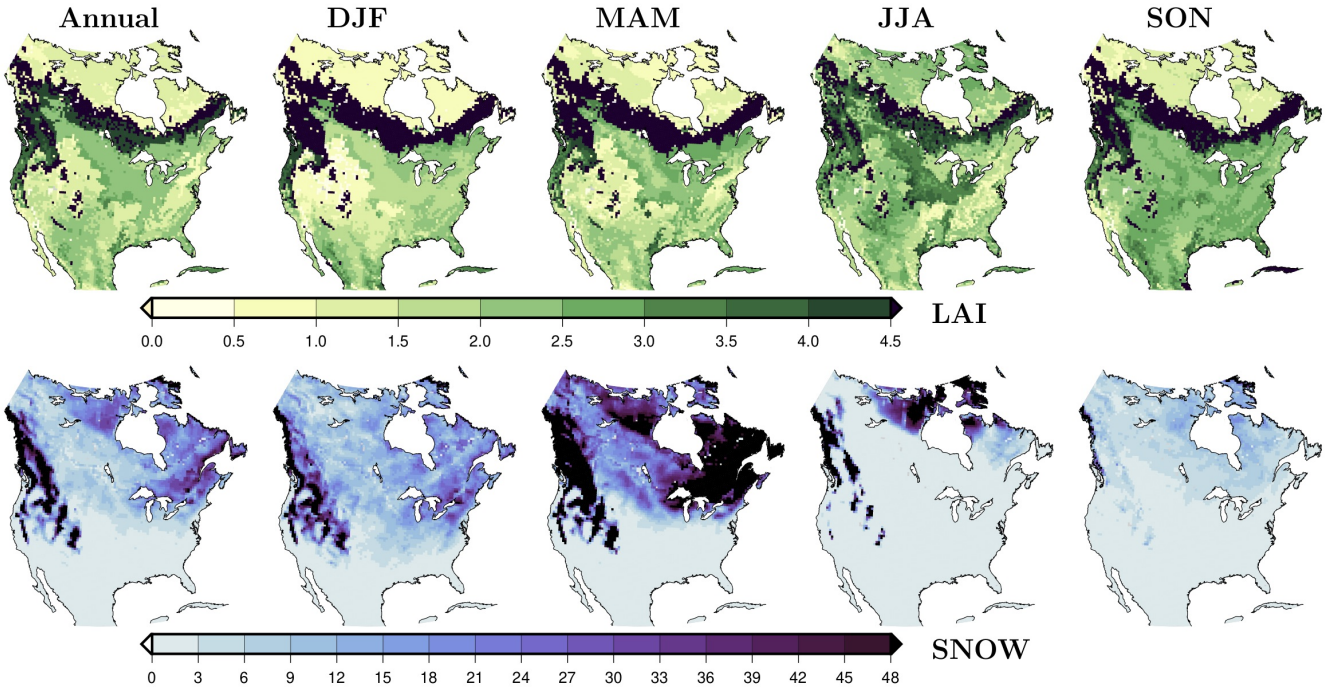

Figure S13. Ranges across the WRF simulations (i.e., difference between the highest value and the lowest value of the simulation ensemble at each grid cell) of Leaf Area Index (LAI, m^2/m^2) and snow water equivalent (kgm^2) annually and for each season. The range among simulations is computed using the mean of each index from 1980 to 2012 for each simulation.

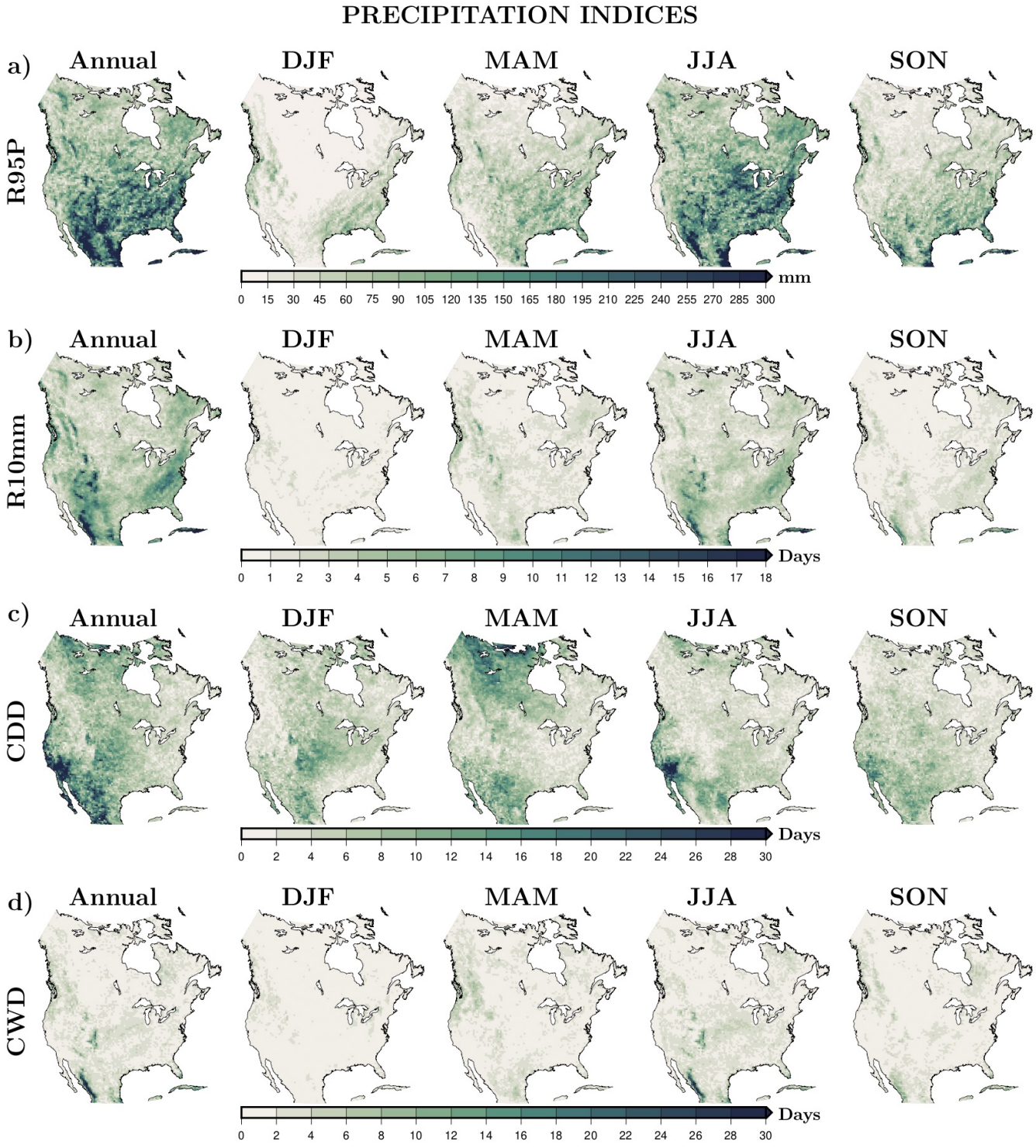

Figure S14. Seasonal component of the multi-model ranges across the WRF simulations (i.e., difference between the highest value and the lowest value of the simulation ensemble at each grid cell) for extreme indices associated with the intensity, frequency and duration precipitation extremes (Table 2). The range among simulations is computed using the mean of each index from 1980 to 2012 for each simulation.

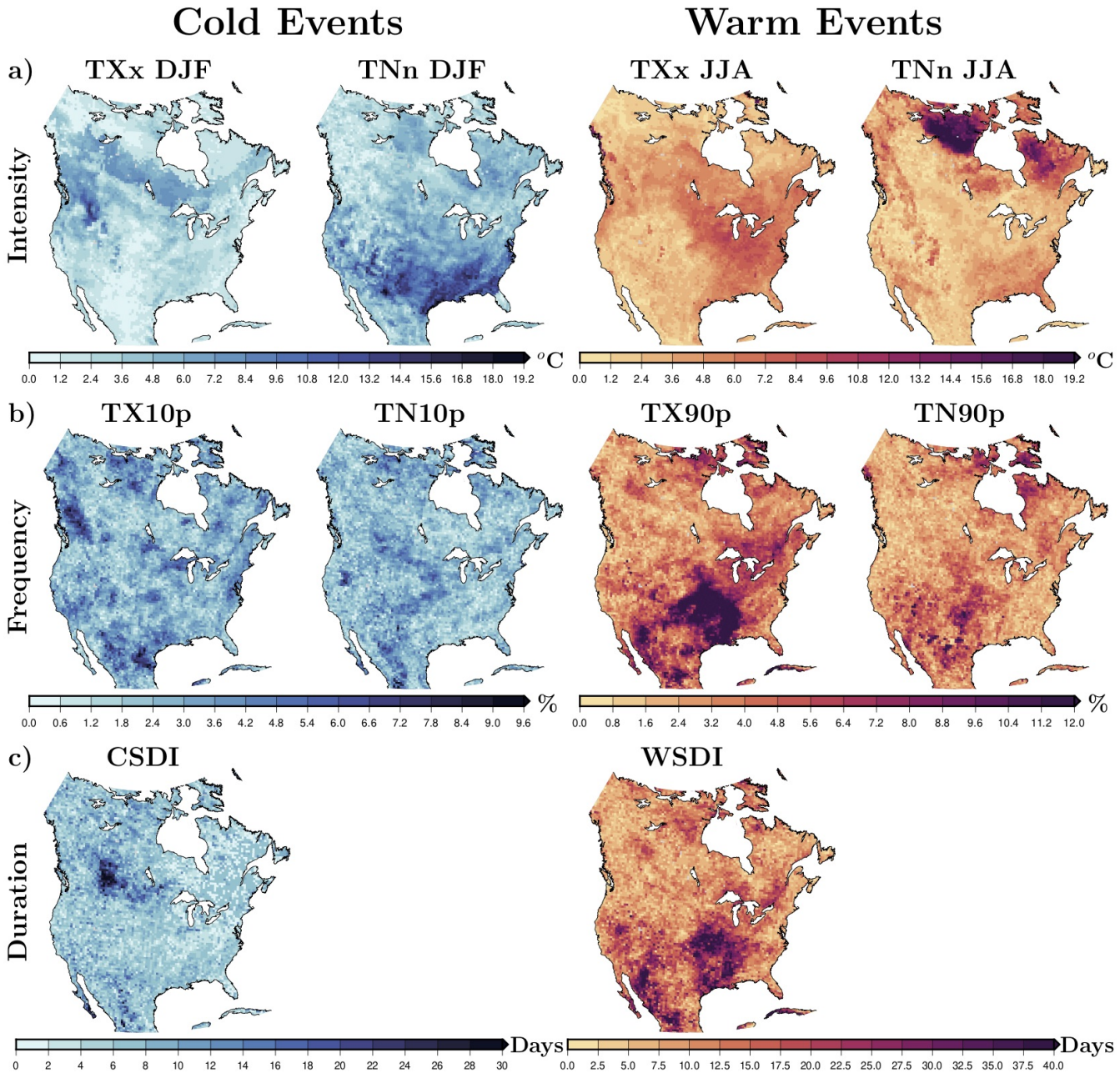

Figure S15. Ranges across the WRF simulations (i.e., difference between the highest value and the lowest value of the simulation ensemble at each grid cell) of extreme indices associated with the intensity (a), frequency (b), and duration (c) of cold (left) and warm (right) extreme temperature events (Table 2). The range among simulations is computed using the 95th percentile of each index from 1980 to 2012 for each simulation, except for the TNnDJF and TNnJJA index for which the 5th percentile of the period was employed.

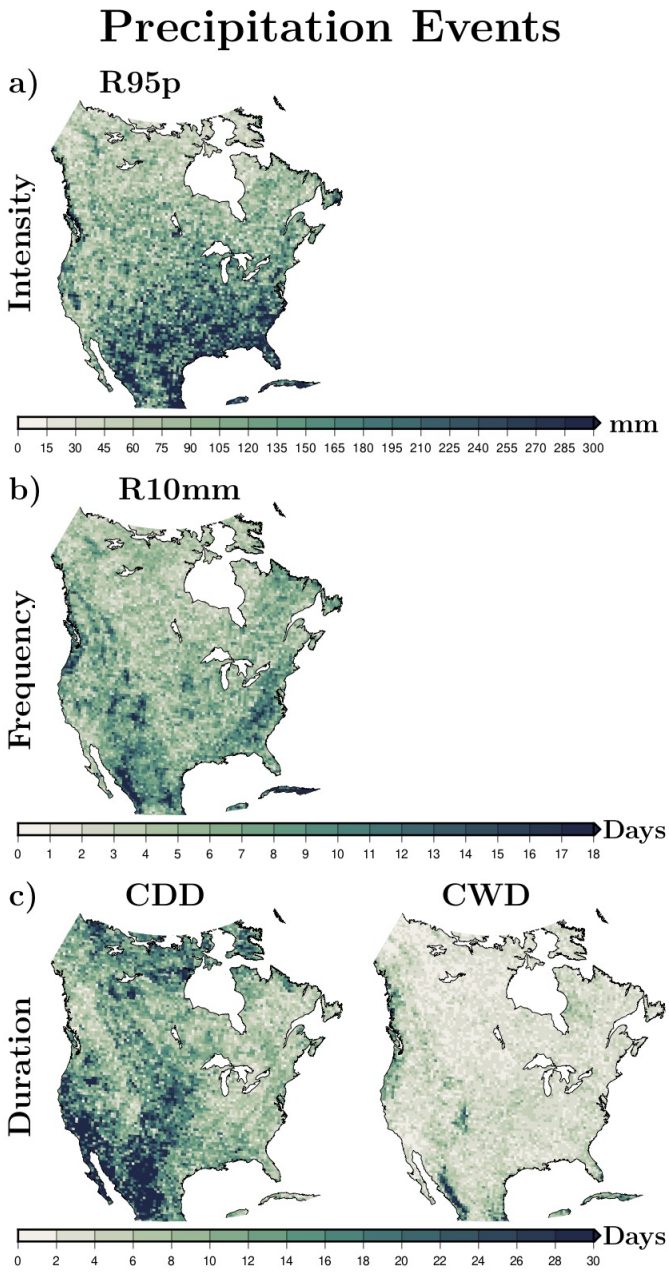

Figure S16. Multi-model ranges across the WRF simulations (i.e., difference between the highest value and the lowest value of the simulation ensemble at each grid cell) of extreme indices associated with the intensity (a), frequency (b), and duration (c) of extreme precipitation events (Table 2). The range among simulations is computed using the 95th percentile of each index from 1980 to 2012 for each simulation.

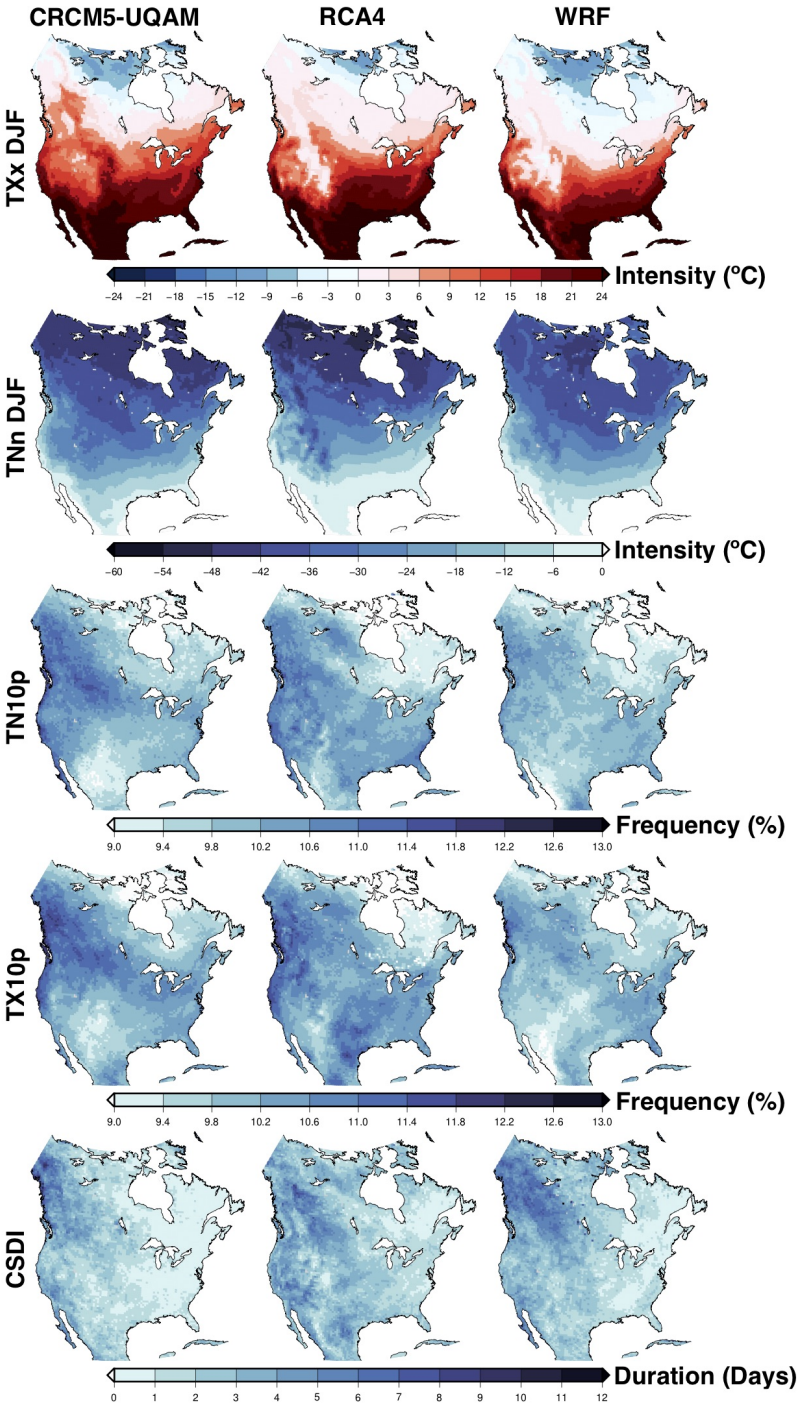

Figure S17. Climatologies of extreme indices associated with intensity, frequency, and duration of cold extreme temperature events for each CORDEX simulation separately (Table 2). The indices are computed using the mean of each index from 1980 to 2012 for each simulation.

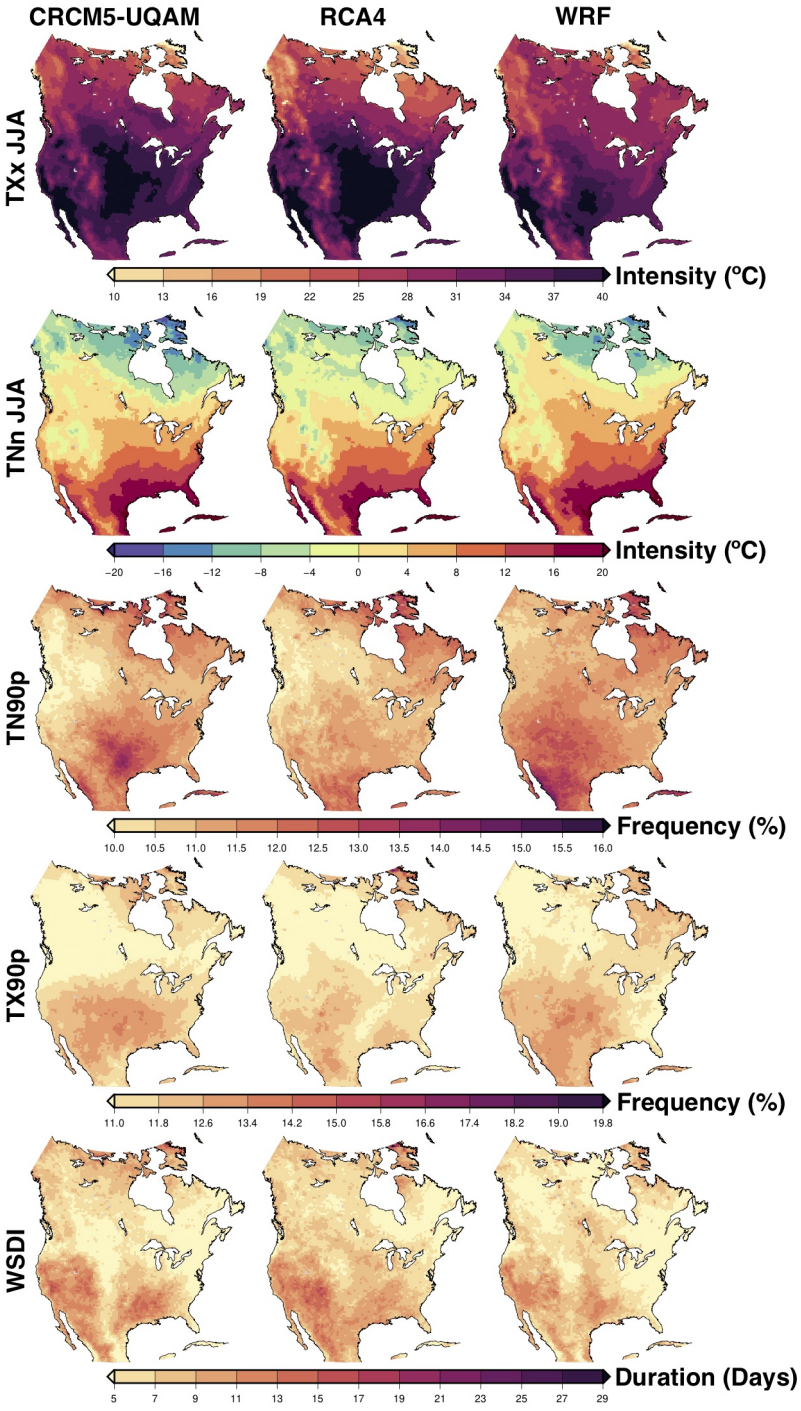

Figure S18. As in Figure S17 but for warm temperature extremes.

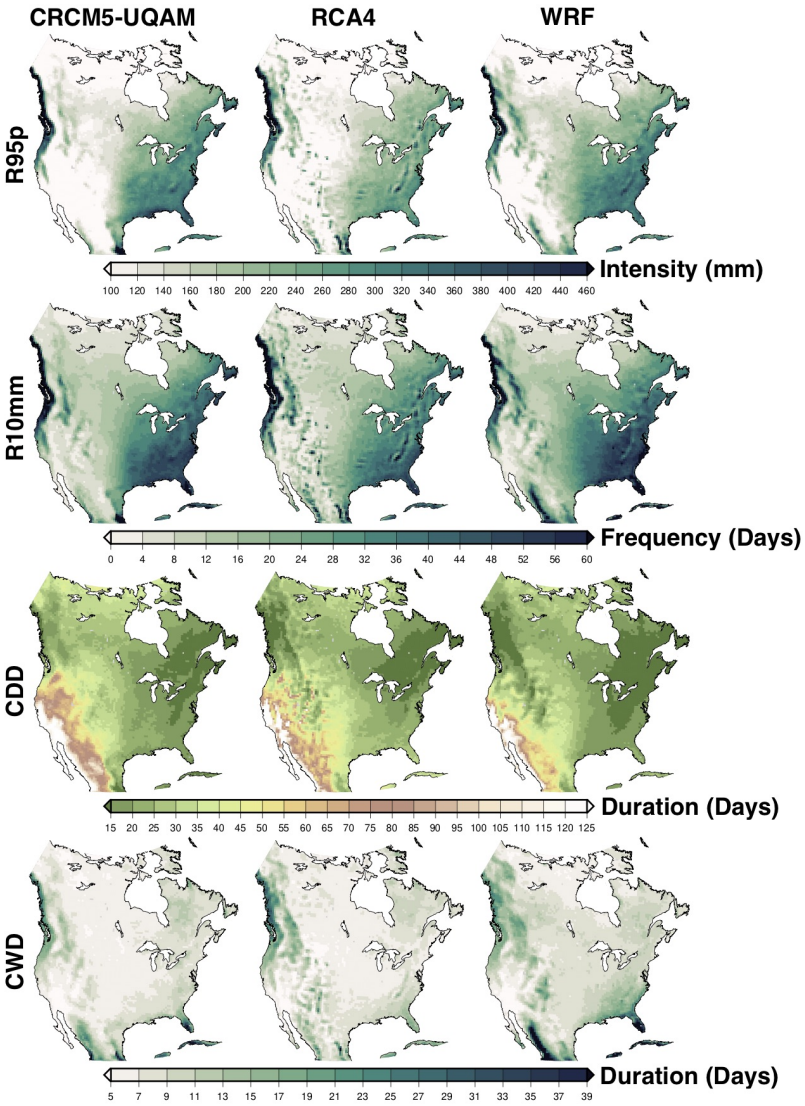

Figure S19. As in Figure S17 but for precipitation extremes.

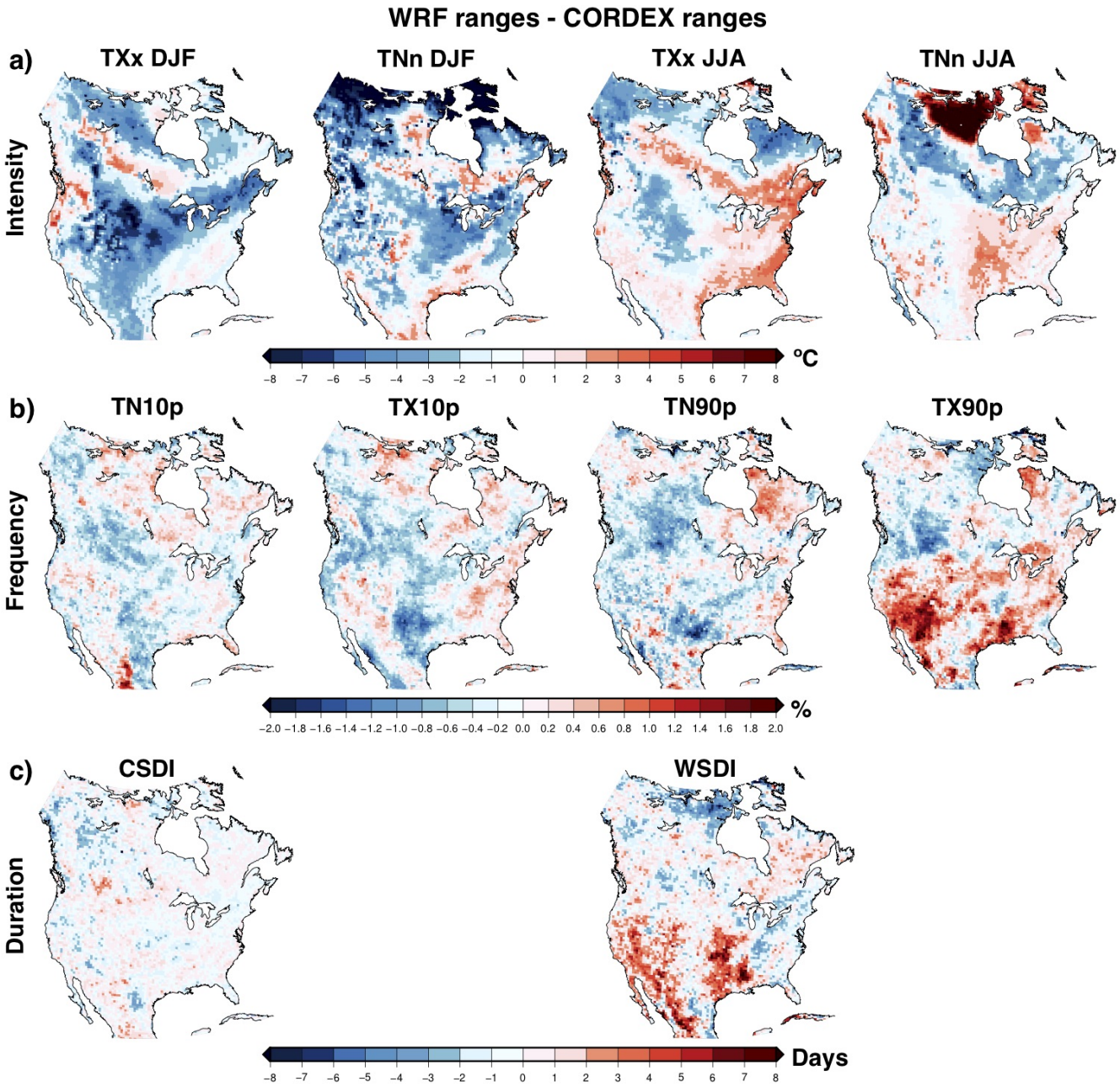

Figure S20. Differences between the range among the WRF simulations and the range among three CORDEX simulations in representing extreme indices related to intensity (a), frequency (b), and duration (b) of cold (left two columns) and warm (right two columns) extreme temperature events (Table 2). Ranges across each simulation ensemble are computed using the mean of each index from 1980 to 2012 for each simulation. Red color means larger rages among the WRF simulations than among the CORDEX simulations, white color means comparable values for ranges among the WRF simulations and the CORDEX simulations and blue color means larger ranges among the CORDEX simulations than among the WRF simulations.

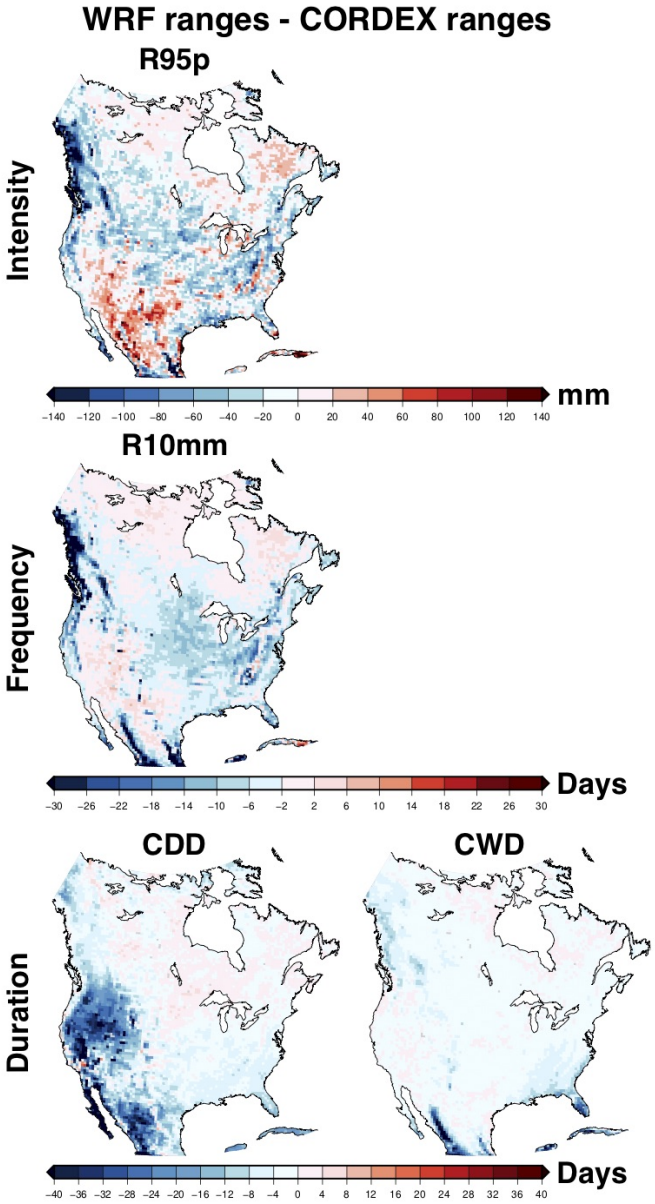

Figure S21. As in Figure S20 but for precipitation extremes.

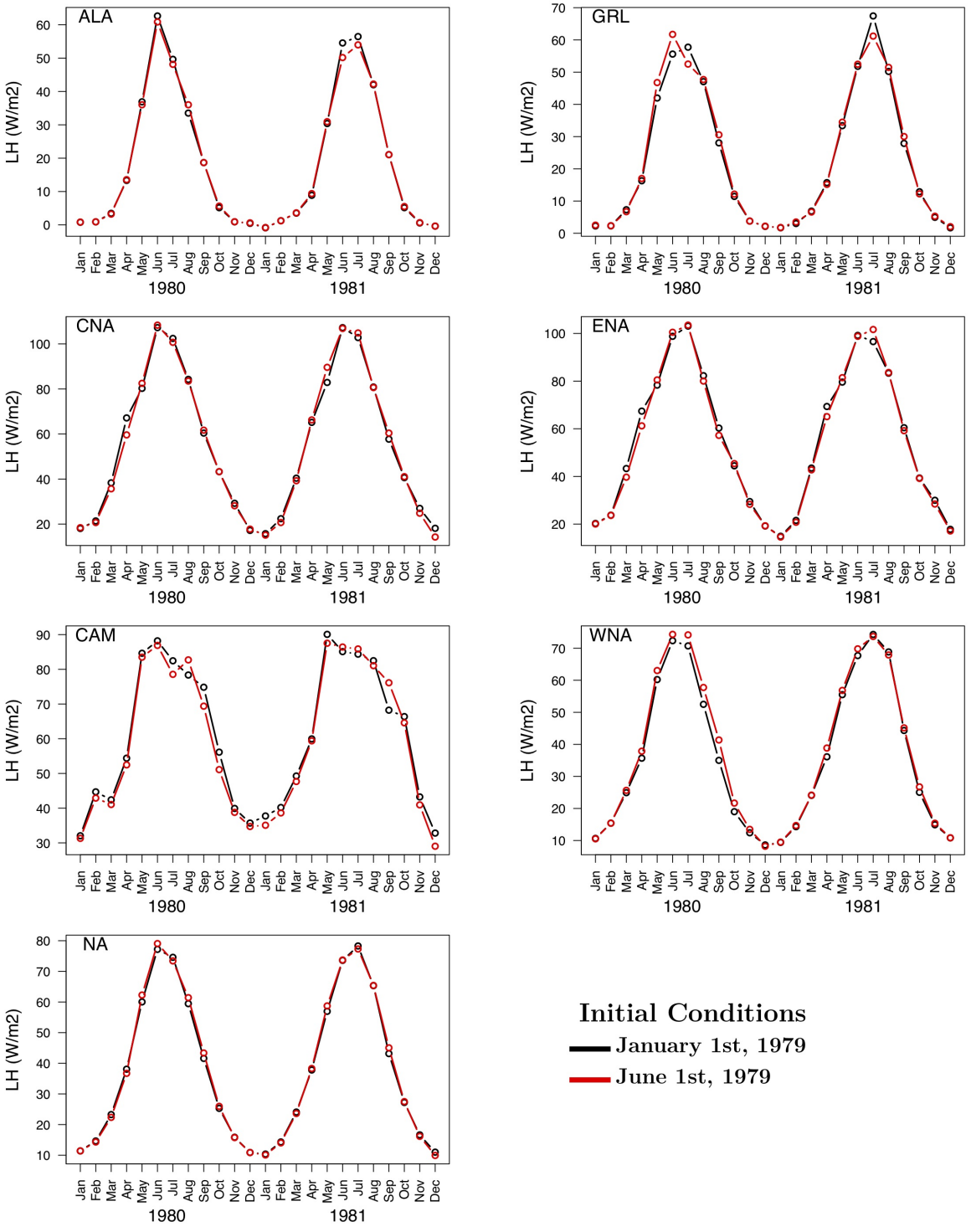

Figure S22. Monthly latent heat (LH) flux from 1980 to 1981 averaged over North America (NA) and the subdomains included in this analysis. The black line represents the outputs from the WRF-CLM4 simulation with initial conditions on January 1st, 1979. The red line represents the outputs from a WRF-CLM4 simulation with initial conditions on June 1st, 1979.

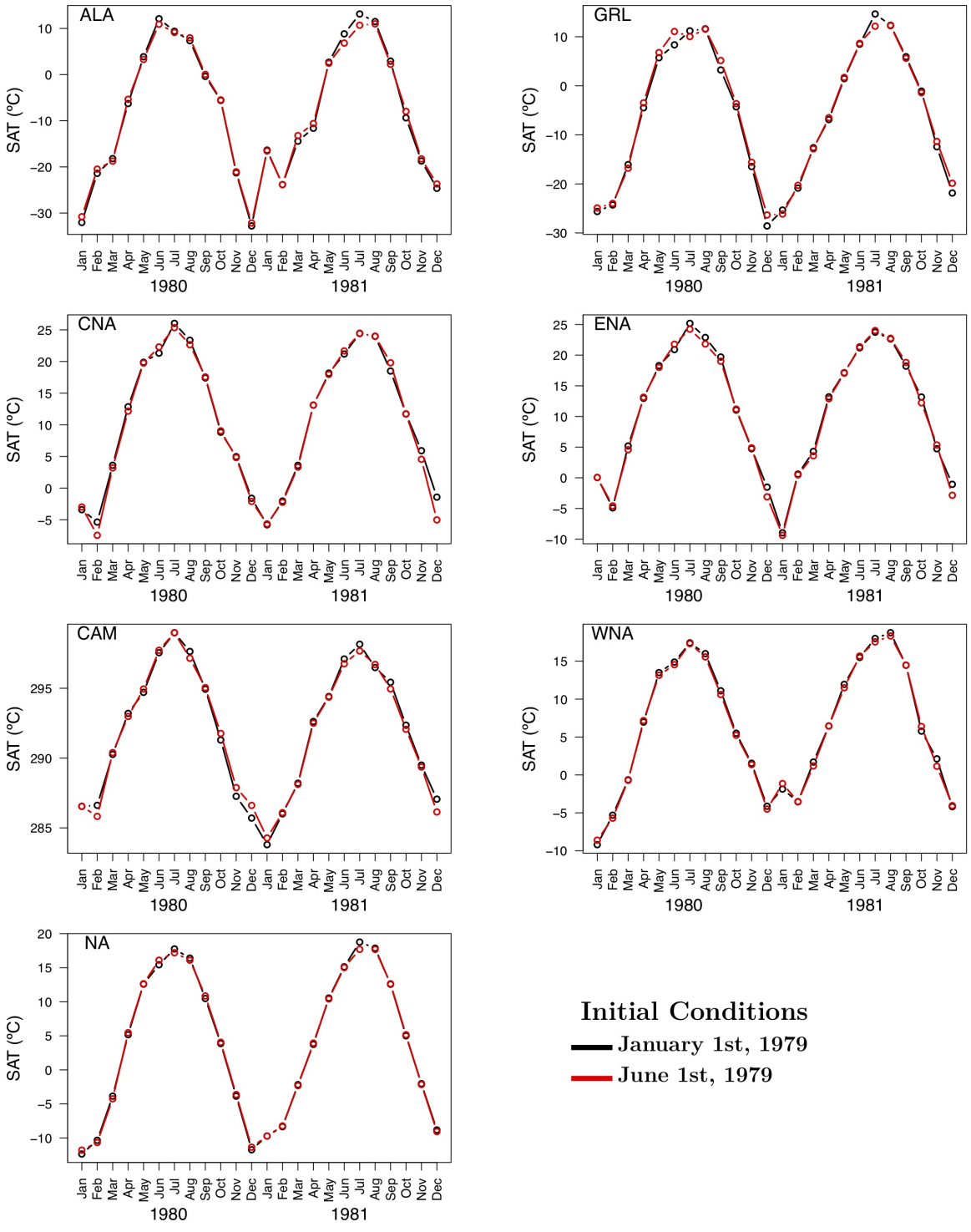

Figure S23. As in Figure S22 but for monthly Surface Air Temperature (SAT).